nature climate change

LETTERS

PUBLISHED ONLINE: 16 MARCH 2015 | DOI: 10.1038/NCLIMATE2569

Effects of long-term variability on projections of twenty-first-century dynamic sea level

Mohammad H. Bordbar[1,2], Thomas Martin[1], Mojib Latif[1,3]* and Wonsun Park[1]

Sea-level rise[1] is one of the most pressing aspects of anthropogenic global warming with far-reaching consequences for coastal societies. However, sea-level rise did[2–7] and will strongly vary from coast to coast[8–10]. Here we investigate the long-term internal variability effects on centennial projections of dynamic sea level (DSL), the local departure from the globally averaged sea level. A large ensemble of global warming integrations has been conducted with a climate model, where each realization was forced by identical CO_2 increase but started from different atmospheric and oceanic initial conditions. In large parts of the mid- and high latitudes, the ensemble spread of the projected centennial DSL trends is of the same order of magnitude as the globally averaged steric sea-level rise, suggesting that internal variability cannot be ignored when assessing twenty-first-century DSL trends. The ensemble spread is considerably reduced in the mid- to high latitudes when only the atmospheric initial conditions differ while keeping the oceanic initial state identical; indicating that centennial DSL projections are strongly dependent on ocean initial conditions.

Globally averaged sea level has risen by about 20 cm since 1900 and at a rate of about 3 mm yr^{-1} during the past two decades, but with strong regional variation[1–7]. For example, the western tropical Pacific featured a much stronger rise than the global average during the recent decades, whereas even falling sea levels were observed in the eastern tropical Pacific and along the west coast of the Americas[7]. Dynamic sea surface topography, the departure from the Earth's geoid, is influenced by ocean currents, local mass balance and density changes of the water column[11–14]. The DSL, which is the focus of this study, has been introduced to describe the collective effect of the local steric (thermosteric and halosteric) and dynamical ocean adjustment contribution[9,11,14]. As the observed sea-level changes include the effects of both external forcing (natural, for example, solar; and anthropogenic, for example, CO_2) and internal variability, we need to understand both drivers to assess twentieth and twenty-first-century sea-level changes.

Climate modes, patterns with identifiable characteristics and specific regional effects, are prominent examples of internal variability. The El Niño/Southern Oscillation[15], a quasi-periodic fluctuation of the equatorial Pacific sea surface temperature with a period of about 4 years, is the leading mode of tropical interannual variability. El Niño/Southern Oscillation is associated with zonal redistributions of heat, causing large sea-level anomalies across the equatorial Pacific and along the west coasts of the Americas[15]. The Pacific Decadal Oscillation, a decadal climate mode, also strongly affects sea level in the Pacific[2,16,17] and tropical South Indian Ocean[18]. Other regions of strong internal decadal sea-level variations are the North[19,20] and South Atlantic[19]. Here we address the influence of the longer centennial variability[21–25] on DSL projections for the twenty-first century. To this end we investigate five large ensembles of global warming integrations with climate models.

We first discuss two ensembles performed with the Kiel Climate Model[24–26] (KCM, Methods). The annual-mean DSL climatology from a millennial control run with fixed atmospheric CO_2 (348 ppm) depicts the well-known features of the large-scale ocean circulation (Fig. 1a), and the pattern is in good agreement with that derived from satellite altimetry (Fig. 1b). However, there are noticeable biases. For example, the 'northwest corner' southeast of Newfoundland is missing and the North Atlantic subpolar gyre extends too far to the east (Fig. 1), which may influence the pattern of forced DSL changes near the east coast of North America and in the North Atlantic. Both ensembles conducted with the KCM consist of 22 global warming integrations, where each ensemble member was forced by increasing atmospheric CO_2 at a rate of 1% per year (compound), approximately corresponding to the observed present rate of increase. Each ensemble member was integrated for 100 years. CO_2 doubling is reached after about 70 years, and the integrations were continued for another 30 years with constant CO_2. The ensemble-mean response is a measure of the CO_2-forced signal, whereas the ensemble spread reflects the effects of internal variability.

In the first KCM ensemble, the individual members start from different atmospheric and oceanic initial conditions that were taken from the above-mentioned unforced control integration and cover a wide range of climate states (Supplementary Fig. 1). The globally averaged ensemble-mean steric sea-level rise amounts to about 0.25 m per century, with only very little spread (Supplementary Fig. 2). We next computed from all ensemble members at each month the globally averaged sea level and subtracted it at each grid point to obtain the time evolution of DSL. The pattern of the ensemble-mean centennial DSL trends (Fig. 2a) depicts strong regional variation. For example, in parts of the Southern Ocean, a drop with a rate of about −0.4 m per century is projected, whereas DSL increases in the mid-latitude North Atlantic by about the same magnitude. The former is related to an enhanced meridional gradient across the Antarctic Circumpolar Current that intensifies in response to stronger surface westerlies, the latter to slowing of the Atlantic Meridional Overturning Circulation. In the tropical and subtropical Pacific, an enhanced zonal asymmetry is projected, consistent with an intensified low-level atmospheric circulation[27,28]. Clearly, the projected centennial trends in DSL can be of the same order of magnitude or even larger than the globally averaged steric sea-level rise in several regions, which is consistent with previous model studies[9,10].

The long-term internal variability effect on projected centennial DSL trends is estimated from the ensemble spread (Fig. 2c,d). Considering the first ensemble (Fig. 2c), in which both oceanic and

[1]GEOMAR Helmholtz Centre for Ocean Research Kiel, Düsternbrooker Weg 20, D-24105 Kiel, Germany. [2]Physics Department, University of Isfahan, Isfahan 81746, Iran. [3]Christian-Albrechts University of Kiel, D-24098 Kiel, Germany. *e-mail: mlatif@geomar.de

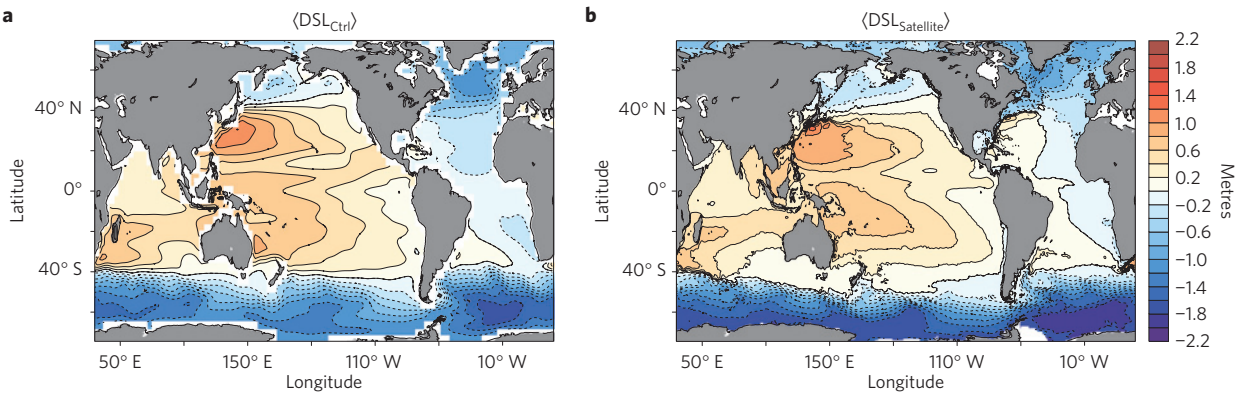

Figure 1 | Comparison of the KCM's DSL, the local deviation from the global average sea level, with satellite observations. a,**b**, The climatological annual-mean DSL computed from the 1,000-yr-long control run with the KCM (**a**) and satellite altimetry during 1993–2012 (**b**). The altimeter-derived sea levels refer to the ocean topography with respect to the geoid and the corresponding DSL map was obtained by removing the spatial average.

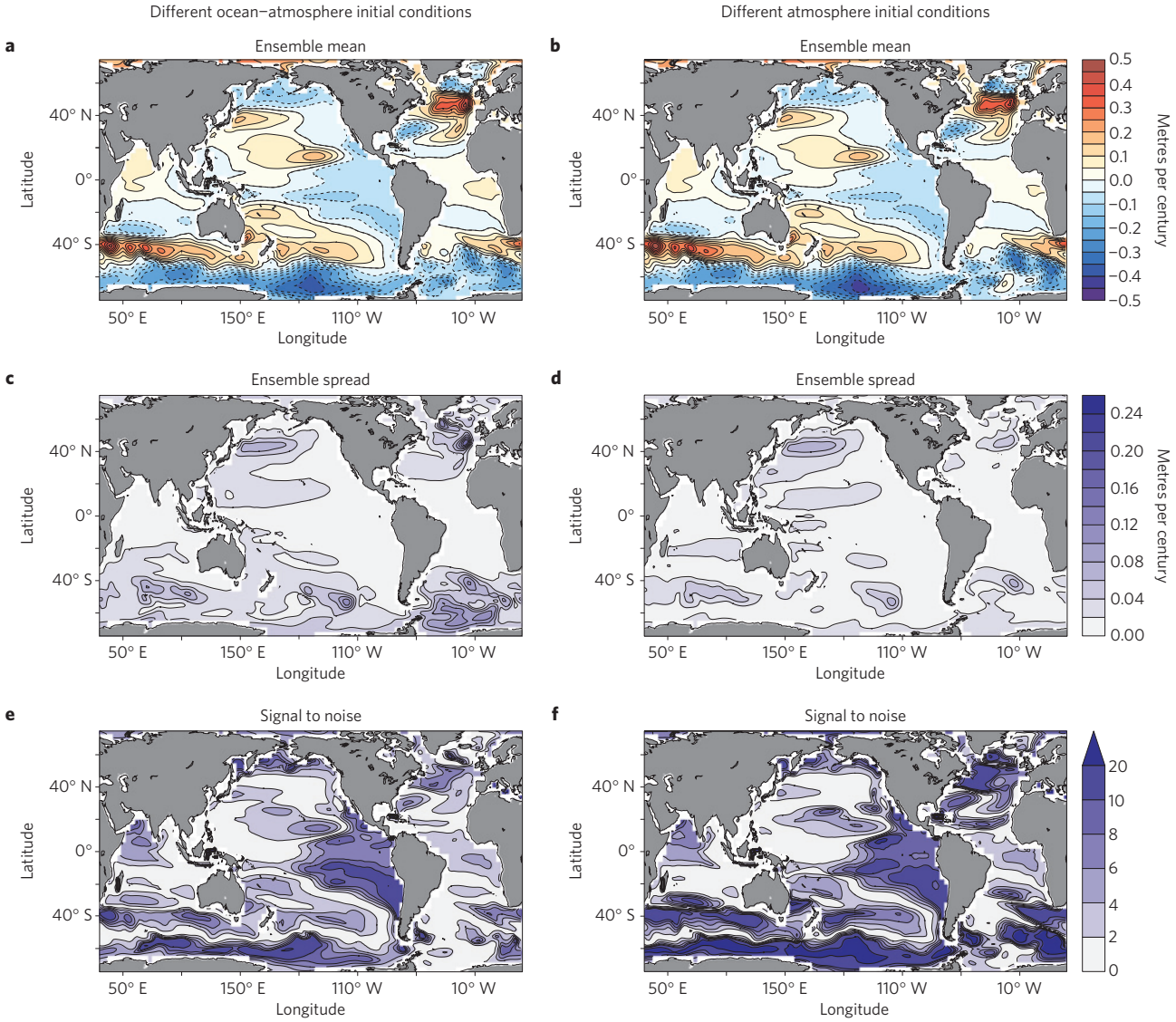

Figure 2 | Long-term internal variability strongly influences centennial DSL projections in the KCM. a,**b**, Ensemble-mean DSL centennial trends. **c**,**d**, Corresponding ensemble spread measured by the standard deviation of the centennial DSL trends calculated from the individual ensemble members. **e**,**f**, Signal-to-noise ratio (the magnitude of the ensemble-mean trends divided by the ensemble spread). All panels are calculated from the 22 global warming integrations-**a**,**c** and **e** have different oceanic and atmospheric initializations, and **b**,**d** and **f** have oceanic initial states are identical and only atmospheric initial conditions vary.

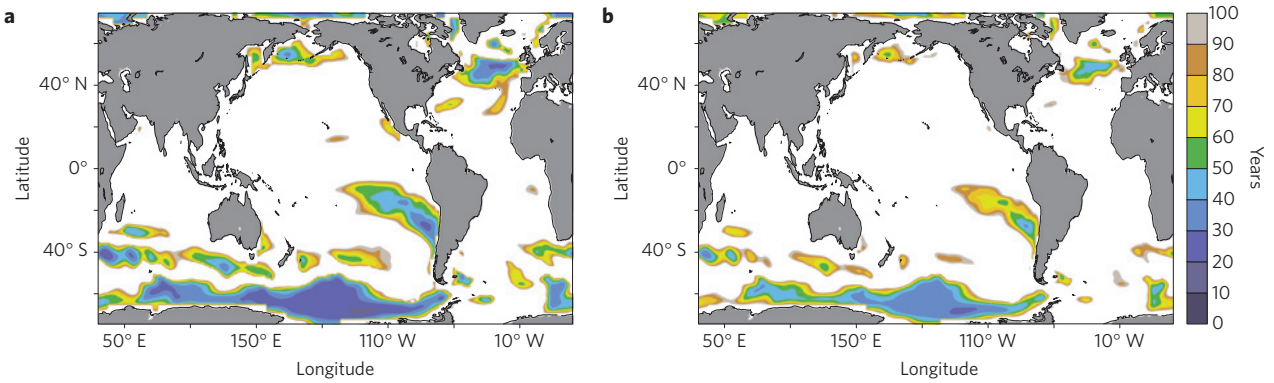

Figure 3 | Detection time of the CO_2 forcing on DSL. a,b, Long-term internal variability can strongly mask the effects of CO_2 forcing even on a centennial timescale. The detection time is defined as the ensemble mean of the times in the individual realizations, when changes associated with centennial DSL trend exceed 2 (**a**) or 3 (**b**) standard deviations of the monthly mean DSL anomalies computed from the control run. White colour denotes detection times longer than a century. DSL is defined as the deviation from the global average.

atmospheric initial conditions vary, the largest spread exceeding 0.1 m per century is found in the mid- and high latitudes, the regions of high internal decadal to centennial variability in the KCM and most other climate models[29]. Calculation of upper- (0–1,830 m) and deep-ocean (1,830 m–bottom) contributions to the centennial steric sea-level trends (Supplementary Figs 3a and 4a) reveals that the deep ocean plays an important role in the Atlantic and Indian Ocean sectors of the Southern Ocean and North Atlantic. The ensemble spread (Supplementary Figs 3b and 4b) is small in the tropics where climate models generally depict strong interannual variability, but weaker decadal to centennial variability[29] (see also Supplementary Fig. 1). An exception is the subtropical west Pacific (Fig. 2c).

The signal-to-noise ratio (Fig. 2e), defined as the ratio of the ensemble mean (Fig. 2a) and ensemble spread (Fig. 2c), is particularly high in four regions: the Southern Ocean, the tropical and subtropical east Pacific, and the mid-latitude North Atlantic and North Pacific. Here the signal-to-noise ratio can locally exceed values of 10, indicating robust CO_2-forced centennial DSL trends. To estimate a 'detection time', the time at which the CO_2-forced DSL signal starts dominating internal variability, we calculated the time when the change associated with the centennial DSL trend exceeds 2 or 3 standard deviations (σ) of the monthly mean sea-level anomalies simulated in the control run. The computation was performed for each ensemble member separately, and the resulting detection times were averaged to obtain an ensemble-mean detection time (Fig. 3). The use of annual or decadal means in the computation of the standard deviations does not fundamentally alter the detection time pattern (not shown) but yields shorter values, meaning that the forced response emerges earlier from the background noise. When considering the 2σ threshold (Fig. 3a), the detection times are longer than a century in most of the world ocean (the white regions), which highlights the important role of long-term internal variability in masking CO_2-forced centennial DSL trends. Exceptions are the regions of high signal-to-noise ratio (Fig. 2e): the Southern Ocean, the tropical and subtropical southeast Pacific and the mid-latitude North Atlantic and northern North Pacific, with detection times of only a few decades in localized regions. The general picture does not change much when the 3σ threshold is applied (Fig. 3b). Overall, the pattern of detection times is similar to that obtained from the Coupled Model Intercomparison Project Phase 5 (CMIP5) model spread[30], but with generally shorter detection times in this study.

Obviously, internal variability introduces large uncertainty to centennial DSL projections in many regions. Is this uncertainty of atmospheric or oceanic origin? To investigate this question, we analyse the second KCM ensemble in which only atmospheric initial conditions differ between members. This assumes perfect knowledge of the oceanic initial conditions and that uncertainty solely originates from the effects of unpredictable weather noise, which would inherently limit DSL predictability. The same methodology has been applied in a previous study addressing DSL projection uncertainty on decadal to multidecadal timescales[31]. The ensemble-mean DSL trend pattern does hardly change (Fig. 2b), but the corresponding ensemble spread is considerably reduced in the North Atlantic and Southern Ocean (Fig. 2d), indicating in these regions a large ocean initial condition contribution to the spread in the first ensemble (Fig. 2c and Supplementary Fig. 5). Consequently, the signal-to-noise ratio becomes larger in these two regions (Fig. 2f).

We now consider the linear DSL trends projected by the CMIP5 models (Supplementary Table 1) applying three future scenarios: Representative Concentration Pathway (RCP) 4.5, RCP 8.5 and 1% CO_2. The three ensemble-mean DSL trend patterns (Fig. 4a–c) are similar to the KCM trend pattern (Fig. 2a) concerning gross features and exhibit high pattern correlations (Supplementary Table 2), especially when considering the two CMIP5 ensembles employing strong forcing (RCP 8.5 and 1% CO_2). There are also noticeable differences. This is expected because the models employ different physical parameterizations and numerical schemes. Consistent with the KCM results, the projected CMIP5-DSL trend patterns depict an enhanced meridional gradient across the Antarctic Circumpolar Current, an enhanced zonal asymmetry in the tropical and subtropical Pacific, and strong positive trends in the mid-latitude North Atlantic.

Spreads computed from multi-model ensembles such as CMIP5 have contributions not only from internal variability but also from model uncertainty. Yet the patterns computed from the three CMIP5 ensembles (Fig. 4d–f) are rather similar to the spread pattern obtained from the KCM (Fig. 2c) depicting low values in the tropics and large values in the Southern Ocean, North Pacific and North Atlantic. This consistency (Supplementary Table 2) also suggests an important contribution of internal variability to the total projection uncertainty in the CMIP5 ensembles. In fact, multiple realizations from six CMIP5 models (Supplementary Table 1 and Supplementary Fig. 6) exhibit large spread in the same ocean regions as the KCM (Fig. 2c). Signal-to-noise ratios calculated from the three CMIP5 ensembles (Fig. 4g–i) are generally smaller relative to those obtained from the KCM (Fig. 2e), but individual CMIP5 models exhibit signal-to-noise ratios consistent with those from the KCM (Supplementary Fig. 6). Comparison of Fig. 4e with the middle panels of Supplementary Fig. 6 provides some information about the relative contributions of initial condition and model uncertainty

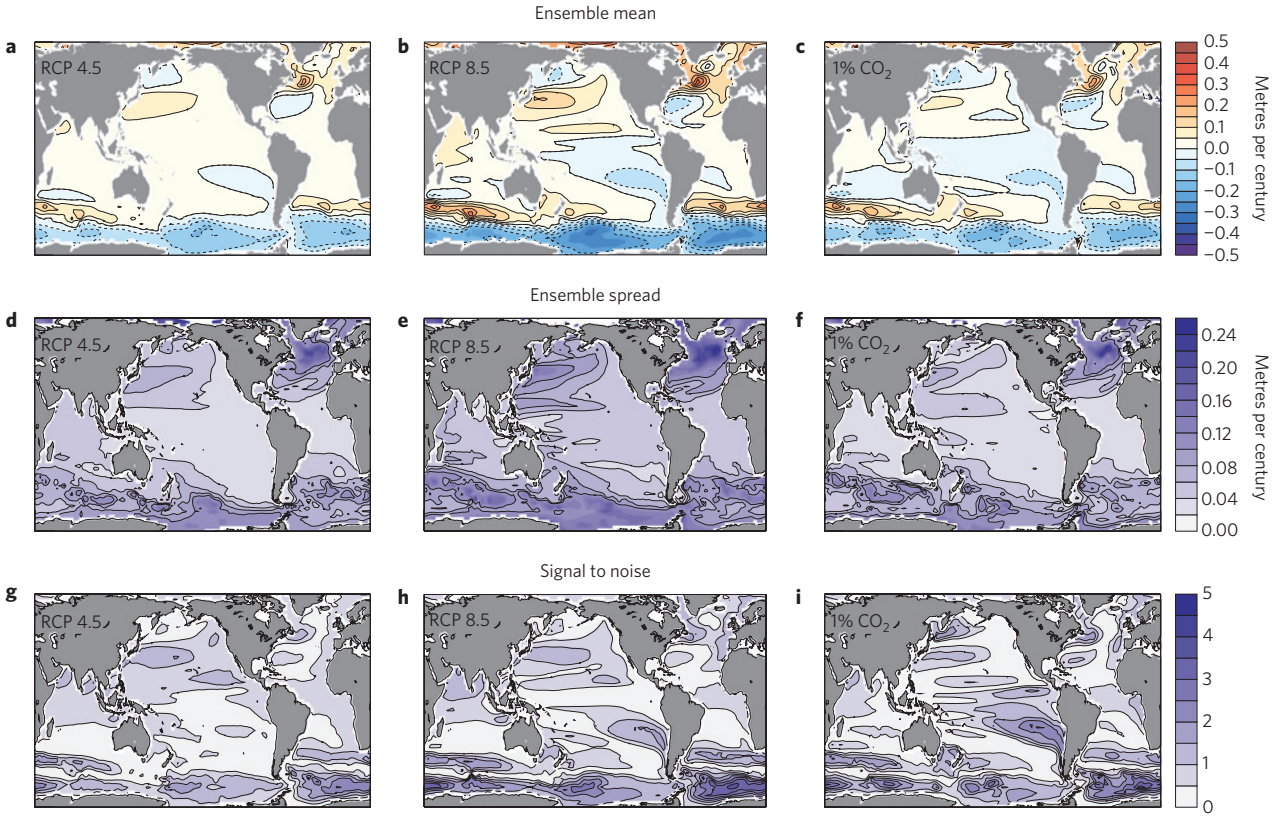

Figure 4 | Results from three CMIP5 ensembles support the finding of a strong influence of long-term internal variability on centennial DSL projections. **a**–**c**, Ensemble-mean centennial DSL trends. **d**–**f**, The ensemble spread measured by the standard deviation of the DSL trends (metres per century). **g**–**i**, The signal-to-noise ratio. **a**,**d**,**g** depict results from the RCP 4.5 (2005–2100), **b**,**e**,**h** from the RCP 8.5 (2005–2100), and **c**,**f**,**i** from the 1% CO_2 (100 years) projections. Note that the colour scale in **g**–**i** is different from that in Fig. 2e,f.

to the total uncertainty. Clearly, model uncertainty seems to be important in many regions but is not the focus of this study. The Southern Ocean seems to be a region of favourable signal-to-noise ratio in both the KCM and CMIP5 models. However, the rectifying effects of mesoscale eddies[32] in the ocean response to intensifying westerlies are not resolved by most climate models. We therefore speculate that the signal-to-noise-ratio in the Southern Ocean may be overestimated by current climate models.

Long-term internal variability considerably influences centennial projections of DSL in many regions of the world ocean, introducing uncertainty about the future evolution in regional sea level. Our findings suggest that this uncertainty can be reduced, especially in mid- to high latitudes, when initializing climate models with ocean state estimates that are consistent with past radiative forcing. The lack of ocean observations, especially during the twentieth century, and model bias, however, make this a challenge. This study suggests an extension of the global ocean observing system to below 2,000 m (Supplementary Fig. 4), as the abyssal ocean is an important source region of centennial variability[9,33]. Future sea-level rise will probably contain increasing contributions from land ice melt which was already contributing the largest share to globally averaged sea-level rise during 1993–2010 (ref. 34). Thus, the importance of DSL relative to the global average sea level may change during the twenty-first century.

Methods

The KCM (ref. 26) consists of the European Centre for Medium-Range Weather Forecasts Hamburg atmospheric general circulation model version 5 (ECHAM5) on a T31 horizontal grid (3.75° × 3.75°) with 19 vertical levels, which is coupled through the Ocean Atmosphere Sea Ice Soil (OASIS) coupler to the Nucleus for European Modeling of the Ocean (NEMO) ocean–sea ice general circulation model on a 2° Mercator mesh amounting on average to 1.3°. Enhanced meridional resolution of 0.5° is employed in the equatorial region and the ocean model is run with 31 levels. No form of flux correction or anomaly coupling is used. For the computation of sea level, see ref. 35. The KCM simulates internal climate variability on interannual, decadal and centennial timescales that is consistent with observations[26,36]. Initial conditions for the greenhouse warming integrations were chosen from a millennial control run, which covers a wide range of climate states (Supplementary Fig. 1).

Mean DSL averaged over 1993–2012 (used for model verification, Fig. 1) are from Archiving, Validation and Interpretation of Satellite Oceanographic data (AVISO; https://icdc.zmaw.de/ssh_aviso.html). In addition, sea levels from climate projections for the twenty-first century supplied by CMIP5 (ref. 37) were analysed (http://cmip-pcmdi.llnl.gov/cmip5/, Supplementary Table 1). The data were interpolated onto a 2° × 2° grid. As in the KCM, the CMIP5 projections do not consider the impacts of land ice melting or vertical land motion. Results from two RCPs are presented: RCP 4.5 and RCP 8.5 denoting a radiative forcing of 4.5 W m^{-2} and 8.5 W m^{-2} by 2100 relative to 1800, respectively. In addition, CMIP5 results are shown where the CO_2 concentration increases by 1% yr^{-1}. We note that the CO_2 concentration in the CMIP5-1% CO_2 scenario is continuously increasing, unlike in the KCM experiments where CO_2 is kept constant after doubling.

Received 17 December 2014; accepted 1 February 2015; published online 16 March 2015

References

1. Church, J. A. & White, N. J. Sea-level rise from the late 19th to the early 21st century. *Surv. Geophys.* **32,** 585–602 (2011).
2. Zhang, X. & Church, J. A. Sea level trends, interannual and decadal variability in the Pacific Ocean. *Geophys. Res. Lett.* **39,** L21701 (2012).
3. Merrifield, M. A. A shift in western tropical Pacific sea level trends during the 1990s. *J. Clim.* **24,** 4126–4138 (2011).
4. Meyssignac, B. & Cazenave, A. Sea level: A review of present-day and recent-past changes and variability. *J. Geodyn.* **58,** 96–109 (2012).

5. Qiu, B. & Chen, S. Multidecadal sea level and gyre circulation variability in the northwestern tropical Pacific Ocean. *J. Phys. Oceanogr.* **42,** 193–206 (2012).
6. Church, J. A. *et al.* Estimates of the regional distribution of sea level rise over the 1950–2000 period. *J. Clim.* **17,** 2609–2625 (2004).
7. Stammer, D. *et al.* Causes for contemporary regional sea level changes. *Annu. Rev. Mar. Sci.* **5,** 21–46 (2013).
8. Church, J. A. *et al.* in *Climate Change 2013: The Physical Science Basis* (eds Stocker, T. F. *et al.*) Ch. 13, 1137–1216 (Cambridge Univ. Press, 2013).
9. Yin, J., Griffies, S. M. & Stouffer, R. J. Spatial variability of sea level rise in twenty-first century projections. *J. Clim.* **23,** 4585–4607 (2010).
10. Yin, J. Century to multi-century sea level rise projections from CMIP5 models. *Geophys. Res. Lett.* **39,** L17709 (2012).
11. Griffies, S. M. & Greatbatch, R. J. Physical processes that impact the evolution of global mean sea level in ocean climate models. *Ocean Modeling* **51,** 37–72 (2012).
12. Gregory, J. *et al.* Twentieth-century global-mean sea-level rise: Is the whole greater than the sum of the parts? *J. Clim.* **26,** 4476–4499 (2012).
13. Cazenave, A. & Remy, F. Sea level and climate: Measurements and causes of changes. *Wiley Interdiscip. Rev. Clim. Change* **2,** 647–662 (2011).
14. Richter, K., Riva, R. E. M. & Drange, H. Impact of self-attraction and loading effects induced by shelf mass loading on projected regional sea level rise. *Geophys. Res. Lett.* **40,** 1144–1148 (2013).
15. Philander, S. G. *El Niño, La Niña, and the Southern Oscillation* (Cambridge Univ. Press, 1990).
16. Hamlington, B. D. *et al.* Uncovering an anthropogenic sea-level rise signal in the Pacific Ocean. *Nature Clim. Change* **4,** 782–785 (2014).
17. Bromirski, P. D. *et al.* Dynamical suppression of sea level rise along the Pacific coast of North America: Indications for imminent acceleration. *J. Geophys. Res.* **116,** C07005 (2011).
18. Schwarzkopf, F. U. & Böning, C. W. Contribution of Pacific wind stress to multi-decadal variations in upper-ocean heat content and sea level in the tropical south Indian Ocean. *Geophys. Res. Lett.* **38,** L12602 (2011).
19. Landerer, F. W., Jungclaus, J. H. & Marotzke, J. Regional dynamic and steric sea level change in response to the IPCC-A1B scenario. *J. Phys. Oceanogr.* **37,** 296–312 (2007).
20. Lorbacher, K. *et al.* Regional patterns of sea level change related to interannual variability and multidecadal trends in the Atlantic meridional overturning circulation. *J. Clim.* **23,** 4243–4254 (2010).
21. Vellinga, M. & Wu, P. Low latitude freshwater influence on centennial variability of the Atlantic Thermohaline circulation. *J. Clim.* **17,** 4498–4511 (2004).
22. Delworth, T. L. & Zeng, F. Multicentennial variability of the Atlantic meridional overturning circulation and its climatic influence in a 4000 year simulation of the GFDL CM2.1 climate model. *Geophys. Res. Lett.* **39,** L13702 (2012).
23. Karnauskas, K. *et al.* A Pacific centennial oscillation predicted by coupled GCMs. *J. Clim.* **25,** 5943–5961 (2012).
24. Latif, M., Martin, T. & Park, W. Southern ocean sector centennial climate variability and recent decadal trends. *J. Clim.* **26,** 7767–7782 (2013).
25. Martin, T., Park, W. & Latif, M. Southern Ocean forcing of the North Atlantic at multi-centennial time scales in the Kiel Climate Model. *Deep Sea Res. II* http://dx.doi.org/10.1016/j.dsr2.2014.01.018 (in the press).
26. Park, W. *et al.* Tropical Pacific climate and its response to global warming in the Kiel climate model. *J. Clim.* **22,** 71–92 (2009).
27. Meng, Q. *et al.* Twentieth century Walker Circulation change: Data analysis and model experiments. *Clim. Dynam.* **38,** 1757–1773 (2012).
28. Solomon, A. & Newman, M. Reconciling disparate 20th century Indo-Pacific ocean temperature trends in the instrumental record. *Nature Clim. Change* **2,** 691–699 (2012).
29. Boer, G. J. & Lambert, S. J. Multi-model decadal potential predictability of precipitation and temperature. *Geophys. Res. Lett.* **35,** L05706 (2008).
30. Lyu, K. *et al.* Time of emergence for regional sea-level change. *Nature Clim. Change* **4,** 1006–1010 (2014).
31. Hu, A. & Deser, C. Uncertainty in future regional sea level rise due to internal climate variability. *Geophys. Res. Lett.* **40,** 2768–2772 (2013).
32. Böning, C. W. *et al.* The response of the Antarctic Circumpolar Current to recent climate change. *Nature Geosci.* **1,** 864–869 (2008).
33. Purkey, S. G. & Johnson, G. C. Warming of global abyssal and deep southern ocean waters between the 1990s and 2000s: Contributions to global heat and sea level rise budgets. *J. Clim.* **23,** 6336–6351 (2010).
34. IPCC in *Climate Change 2013: The Physical Science Basis* (eds Stocker, T. F. *et al.*) (Cambridge Univ. Press, 2013).
35. Roullet, G. & Madec, G. Salt conservation, free surface, and varying levels: A new formulation for ocean general circulation models. *J. Geophys. Res.* **105,** 23927–23942 (2000).
36. Park, W. & Latif, M. Pacific and Atlantic multidecadal variability in the Kiel Climate Model. *Geophys. Res. Lett.* **37,** L24702 (2010).
37. Taylor, K. E., Stouffer, R. J. & Meehl, G. A. An overview of CMIP5 and the experiment design. *Bull. Am. Meteorol. Soc.* **93,** 485–498 (2012).

Acknowledgements

We acknowledge the World Climate Research Programme's Working Group on Coupled Modeling, which is responsible for CMIP, and we thank the climate modelling groups (listed in Supplementary Table 1) for producing and making available their model output. For CMIP the US Department of Energy's Program for Climate Model Diagnosis and Intercomparison provides coordinating support and led development of software infrastructure in partnership with the Global Organization for Earth System Science Portals. The altimeter products were produced by Ssalto/Duacs and distributed by AVISO with support from CNES. This work was supported by the BMBF RACE (No. 03F0651B) and EU FP7 NACLIM (grant agreement no. 308299) Projects. The KCM runs were performed at the Kiel University Computing Center.

Author contributions

M.L. suggested the study, organized the analyses and wrote the first draft of the paper. M.H.B. and T.M. analysed the KCM and CMIP5 data. W.P. co-designed and conducted the KCM experiments and prepared the data for analyses. M.H.B. produced the diagrams. All authors discussed and interpreted the results and implications at all stages.

Additional information

Supplementary information is available in the online version of the paper. Reprints and permissions information is available online at www.nature.com/reprints. Correspondence and requests for materials should be addressed to M.L.

Competing financial interests

The authors declare no competing financial interests.